Optical Field Enhancement at Cusps between Adjacent Nanoapertures

Tiberiu-Dan Onuta, Matthias Waegele, Christopher C. DuFort,
William L. Schaich, and Bogdan Dragnea*

*Departments of Chemistry and Physics, Indiana University,
Bloomington, Indiana 47405*

ABSTRACT

Optical nonlinear properties of cusps formed at the junction between two circular apertures in a metal film have been studied by scanning confocal microscopy. For gold, both second harmonic and broadband emission are enhanced when the pump polarization is directed across the gap between cusps, similar to the behavior of the recently studied bowtie antennas and apertures. However, field enhancements are also present when the polarization is perpendicular to the gap direction. A quantitative explanation of the observed relative signal intensities requires considering both field concentration near cusps and shape resonances of the entire structure. The occurrence of broadband emission from the cusp region when Al is used instead of Au indicates that broadband emission is the result of additional mechanisms besides pure two-photon luminescence.

Introduction. Spatial control of optical near fields remains a key challenge in the development of large-scale integrated plasmonic technologies. One approach to this problem has been to explore whether principles of radio wave antennas can be transferred into the optical realm.[1-3] However, finite metallic conductivity, specifics of the electronic band structure and surface chemistry, and use of high power density light sources represent significant deviations from the classical case of metallic structures at radio frequencies.

Such differences have led to the discovery of new principles for optical antenna design and also to new technological opportunities that have no parallel in classical antenna electromagnetism such as near-field nanolithography,[4-7] superresolution imaging,[8] tip-enhanced Raman spectroscopy,[9-11] and near-field optical manipulation.[12-15]

One of the first structures studied for its enhanced optical near-field properties is the bowtie antenna,[16,17] which is composed of two flat metallic equilateral nanotriangles symmetrically deposited on a transparent substrate so that a narrow gap separates two opposing tips, Figure 1a. Upon illumination, for gaps much smaller than the wavelength, the maximum intensity inside the gap can reach values approximately 3 orders of magnitude larger than the incident field intensity.[18] These strong fields are localized near the tips and therefore well beyond the diffraction limit,[18] hence the interest for superresolution imaging.

For the linear optical properties, a gap-dependent wavelength resonance in the enhancement has been predicted and experimentally found.[19]

In the case of gold nanotriangles and under short pulse laser radiation (~0.1-1.0 ps), a broad continuum is emitted
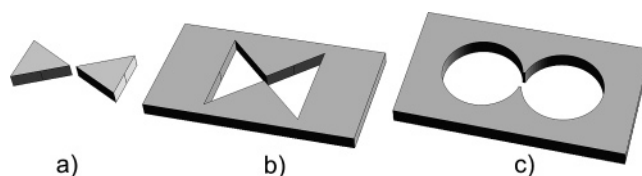
Figure 1. Schematic of several structures for optical near-field enhancement: (a) the bowtie antenna,[18] (b) the bowtie aperture,[20] (c) the cusp structure discussed in this paper.

from near the tips. The origins of this nonlinear optical response remain somewhat unclear, the broadband emission having been associated either with plasmon-assisted two-photon photoluminescence (TPPL) from gold[3] or with white-light supercontinuum (WLSC) emission from the gap region.[2]

A structure that is the complement of a bowtie antenna in the Babinet sense is the bowtie aperture,[20] Figure 1b. The bowtie aperture is interesting for near-field imaging and spectroscopic applications because of its large transmission and reduced background, but its nonlinear optical properties have not been studied yet.

A similar type of near-field optical resonator consists of a double cusp structure between two adjacent apertures in a metal film (Figure 1c).[21] The double-cusp structure has one notable feature that differentiates it from the previous schemes: the circular hole rims should be able to support surface mode oscillations. When such a structure is arranged in an array of coupled apertures, enhanced SHG transmission is observed.[21] Here we study individual cusp antennas and we discuss their field-enhancement properties as revealed by nonlinear optical microscopy and theoretical simulations.

The double-cusp configuration is particularly useful for comparisons of the nonlinear optical properties of the gap region with the well-understood nonlinear optical properties of the surrounding metal film because the structure and the film are made of the same material and share the same fabrication process (thermal evaporation and deposition under vacuum). The present study shows that the mechanism for broadband emission from the gap region differs from that for the surrounding film.

Experimental and Theoretical Section. *Nanosphere Lithography of Hole Pairs.* A variant of the nanosphere lithography technique[22,23] was used for fabricating holes with diameters between 300 and 1000 nm in a gold film evaporatively deposited on silica microscope cover slips. At high polysterene particle concentrations ($>10^{12}$ cm^{-3}), a dynamic population of particle dimers exists. After drying, metal coating, and brief sonication, these dimers leave behind a significant concentration of hole pairs, Figure 1c.

Microscopy and Optical Spectroscopy. AC-mode atomic force microscopy (MFP3D, Asylum Research; Si cantilever, 70 kHz, ~10 nm tip radius) was performed to measure film roughness and cross-sectional profiles of selected cusps. As a more rapid alternative to AFM imaging, albeit at the cost of morphological detail along the normal to the surface, scanning electron microscopy (SEM) was employed. Reflection multiphoton scanning confocal microscopy has been performed on a home-built apparatus composed of a Ti:Sapphire oscillator (Coherent, Mira, 76 MHz repetition rate, 150 fs pulse width, 800 nm wavelength), optical isolator, spatial filter and beam expander, gradient neutral density filter for power adjustments, Nikon 300 TE inverted microscope, 1.4 NA oil 60× CFI objective, Polytec PI piezo stage (RHK SPM 2000 controller), dichroic splitter, photon-counting avalanche photodiode detector (Perkin-Elmer, SPCM-AQR-16-FC) bandpass filtered to collect wavelengths between 550 and 650 nm, photon-counting photomultiplier (Hamamatsu) bandpass filtered at 400 nm, and monochromator (300i, Acton Research) coupled to a photon-counting detector (Perkin-Elmer, SPCM-AQR-16-FC) for spectral analysis. Laser power at the sample was kept in all cases below the known damage threshold for thin gold films, 3 mW/μm^2, which for our configuration corresponds to an incident intensity of 500 μW.

Finite Difference Time Domain Computations. The finite-difference time-domain method (FDTD) is well suited for modeling complex nanostructures.[24] Our code uses a staggered cubic mesh for the field components with a step size of ~8 nm. The incident field is a linearly polarized, Gaussian pulse whose width is a few hundred nanometers. The incident pulse enters (and varies only) along the normal to the film from the glass side. It is introduced by the total field/scattered field technique.[24] To suppress unphysical reflections, the numerical domain is bounded on all sides by perfectly matched layers (PML). These layers begin ~300 nm above and below the gold film. Within the plane of the film, the PML lie outside a square of side ~2.5 μm. We checked that increasing these dimensions does not significantly change the results near the holes.

For the glass substrate, we use a constant index of refraction $n_g = 1.5$, while the gold is described by a Drude dielectric function:

$$\epsilon = \epsilon_d - \epsilon_0 \frac{\omega_p^2}{i\gamma}$$

The three parameters ($\epsilon_d/\epsilon_0 = 8$, h$\omega_p = 8.8$ eV, $\gamma/\omega_p = 0.008$) are chosen to give a reasonable fit to the optical response of gold[25] for wavelengths above 600 nm (i.e., for energies below the interband threshold).

The calculation proceeds by the standard leapfrog time-marching scheme. To perform a spectral analysis, we keep running time-Fourier transforms of selected field components at locations of interest. This readily yields, say, the absolute square of the electric field just outside a cusp as function of incident light wavelength. To determine the more challenging far-field transmission, we need a time- and space-Fourier transform of the near fields in a plane just above the film in vacuum. From this information, a near-to-far field transformation can be done using Green's theorem.[24]

Results. Single apertures provide a convenient reference structure for the study of paired holes. Figure 2 shows for a pump power of 475 μW the spatial distribution of the emission due to either second harmonic generation (SHG) or a broadband continuum. A single pixel in each frame is formed by focusing the incident laser light to a diffraction-limited spot of width 285 nm and collecting the light emitted back from that area onto a 6 μm core optical fiber connected to a photon-counting module. Thus the incident and collected light both propagate in a cone of opening angle 135°, centered on the normal to the film. Moving the sample in raster fashion with fixed optics then generates the whole frame. Both types of emission are enhanced at the edges of a single hole, but the maximum enhancements may be at different locations for SHG or the broadband continuum. For example, the second column of Figure 2 corresponds to a 771 nm diameter aperture, which has an SHG emission maximum on the right side, while the emission maximum for the broadband continuum is on the left side. This difference between the two emissions (measured simultaneously from the same hole) proves that they arise from different physical mechanisms. We also remark that the left−right asymmetries in all the panels of Figure 2 likely arise from fine scale edge roughness or local film thickness variations. Different holes with the same nominal parameters show different asymmetries. This difficulty, which is often seen in nonlinear response (e.g., in surface-enhanced Raman scattering), is also present for pairs of holes. We define the enhancement factor as the ratio between the maximum intensity emitted by the structure and the average intensity emitted by the film, far from the structure. Comparable enhancements (~100) are obtained for both SHG and the broadband continuum.

When scanning a hole pair, the shape of the emission pattern depends on the polarization orientation with respect to the line joining two cusps (cusp line) and on the size of the gap between the two cusp tips. Control of this gap is not
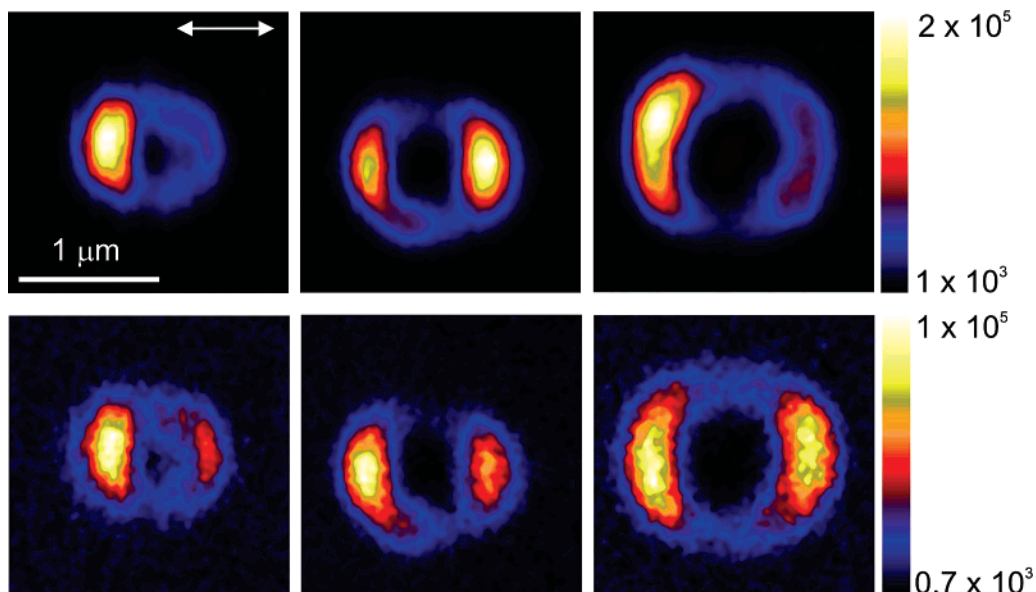
Figure 2. Simultaneously acquired SHG (top row) and broadband continuum (bottom) micrographs of single circular apertures in a gold film. The aperture diameters are: 585, 771, and 1070 nm. The double arrow indicates the electric field polarization.

Table 1. Dependence of Gap on the Film Thickness

film thickness (nm)	100	200	300
gap (nm)	180 ± 20	250 ± 50	400 ± 70

directly achievable by the nanosphere lithography method, but we have observed a systematic dependence of the average gap (measured at the film surface) on the film thickness, Table 1. This variation holds for aperture diameters in the range ∼250−1000 nm, subject to the constraint that the aperture radius be greater than the film thickness.

The film roughness (1.5 nm rms) and the vertical profile were measured by AFM, Figure 3. The AFM-measured wall angle is a convolution between the real angle and the AFM tip angle. The wall angle directly measured from the AFM cross-section (Figure 3b) is 42°. The tip angle (Figure 3b, insert) is 35°. Therefore, the actual wall angle is less than 10°, which is small enough for our purposes to be neglected. Note, however, the left−right asymmetry of the hole profile

Figure 4 shows typical micrographs of aperture pairs for second harmonic and broadband radiation (1070 nm diameter apertures, 450 μW incident power). For polarization parallel to the cusp line, the full width at half-maximum (fwhm) of the most intense region between the cusps is 320 nm, slightly larger than the 285 nm width of the incident light.

Figure 5 shows the spectrum collected from the most intense spot centered between the cusps in the case of parallel polarization. The spectrum has been corrected for the spectral response of the detector and of the monochromator. Broadband continuum emission along the cusp line has a spectral range from 380 nm to beyond 650 nm. The emission from this region is much greater than the luminescence emitted by the film.

The dependence of the broadband and SHG signals on the pump power was measured for light emitted along the cusp line and from the film. All data were least-square fit with a power law with the exponent as a fit parameter. In

the case of the film, both SHG and broadband continuum were satisfactorily fit by a quadratic function (exponent: 2.0 ± 0.1). Near the cusps, the broadband continuum data requires an exponent of 1.9 ± 0.1, which is still quadratic within the experimental error. However, the SHG fit required a superquadratic exponent of 2.4 ± 0.1, Figure 6.

Discussion. SHG is dipole-forbidden in media having an inversion symmetry center, although bulk contributions coming from higher-order multipoles are possible. At an interface between media inversion, symmetry (along the normal) is necessarily broken and surface SHG is enhanced when the incident field polarization is perpendicular to the interface. Furthermore, for a nonflat interface, most of the field enhancement that develops is associated with the locally normal field component, so subsurface emission from quadrupole contributions will also be enhanced. These general properties provide a rationale for the qualitative features of Figure 2. On a smooth film and at normal incidence, the polarization is parallel to the surface (no surface enhancement) and there is negligible surface SHG. Similarly, near a hole, one expects weak signals at locations where the electric field is mostly parallel to the edge of the aperture. As one moves around the hole's rim, the SHG signal should vary as $(\sin \theta)^4$, where θ is the angle formed by the E vector with the local tangent at the edge, Figure 7a. The qualitative agreement between the $(\sin \theta)^4$ function convoluted with a theoretical point spread function characterizing the microscope in Figure 7a and the experimental data from single apertures in Figure 2 suggests that, for our scanning spot experiment, local boundary conditions are dominating the optical response of a single hole.

FDTD computations were used to quantify the fields near a hole edge, Figure 7b. Be careful to note when comparing such calculations with our measurements (both here and below) that we calculate only the linear fields due to normally incident light, while we measure nonlinear fields induced
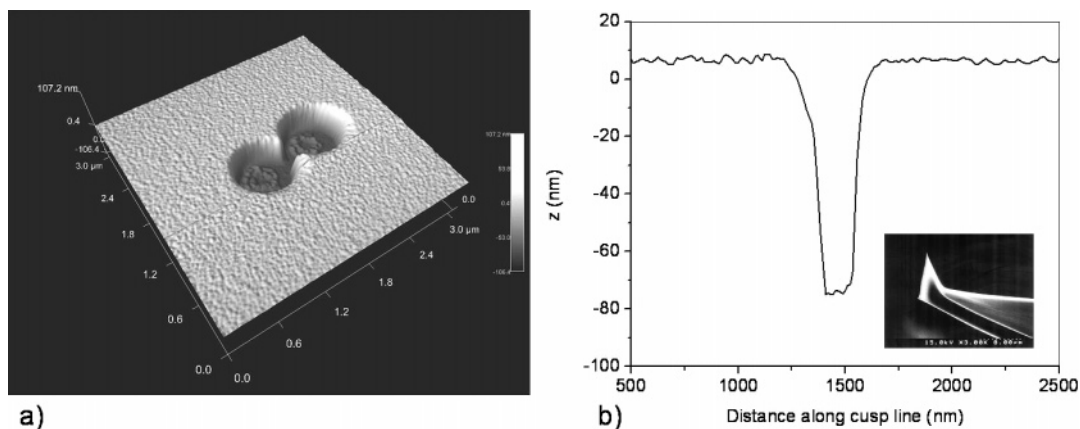
Figure 3. (a) AFM topographic mapping of a pair of adjacent holes. (b) Cross-section along the cusp line for measuring the wall angle and electron micrograph of the tip (inset).
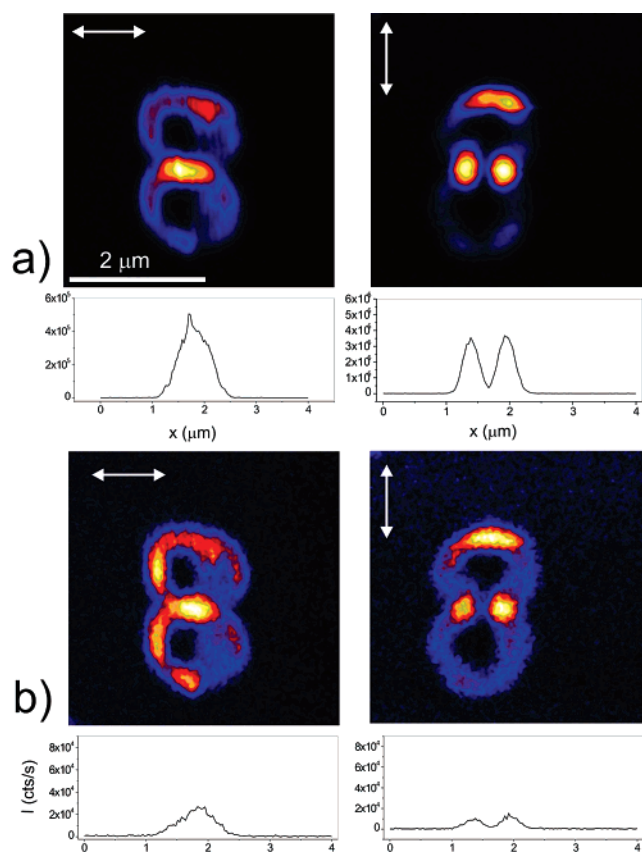
Figure 4. SHG (a) and broadband (b) emission micrographs of a pair of adjacent apertures and signal cross-sections along the cusp line. The incident laser polarization is represented by the double arrow.

Figure 5. Spectrum of the light emitted from either the gap region or the film. The shaded areas represent collection bandwidths for SHG and broadband continuum. The spectra have been corrected for the spectral transmission and sensitivity of the experimental apparatus. The relative size of the gap and film signals is suppressed by the normalization.

by incident fields that converge toward the surface from a wide cone. The maximum field enhancement on the front side of the hole edge is 1.7. The observed ripple in the position of the most intense spots in Figure 7b is due to the discrete nature of the cubic numerical mesh. The localization of the absolute maximum of field enhancement depends on wavelength, the hole diameter, and the film thickness. Because a long attenuation length ($\sim$40 μm at 800 nm) is expected for surface plasmon polaritons on gold, coupling of edge modes may play a role in the optical response.[26] In

our case, for example, the most intense edge enhancement effect is obtained on the back side of the film, not on the front side as for isolated zero-mode waveguides or straight edges.[27]

Turning now to the emission from a pair of holes, the spectra in Figure 4 contain both a narrow SHG peak and a broad feature spanning the entire spectral window of our detector. Single-photon excitation of noble metal surfaces results in little visible photoluminescence,[28] even at frequencies high enough to excite interband transitions. The standard explanation for this inefficiency is that nonradiative energy relaxation mechanisms are much faster than the radiative recombination between electrons near the Fermi level and photoexcited holes in the first d band. However, photoluminescence from small clusters, nanoparticles, or rough noble metal surfaces can be significantly enhanced due to quantum confinement effects on the band structure (for metal clusters smaller than 2−3 nm) or to localized plasmon resonances (for rough surfaces and nanoparticles).[29−31]
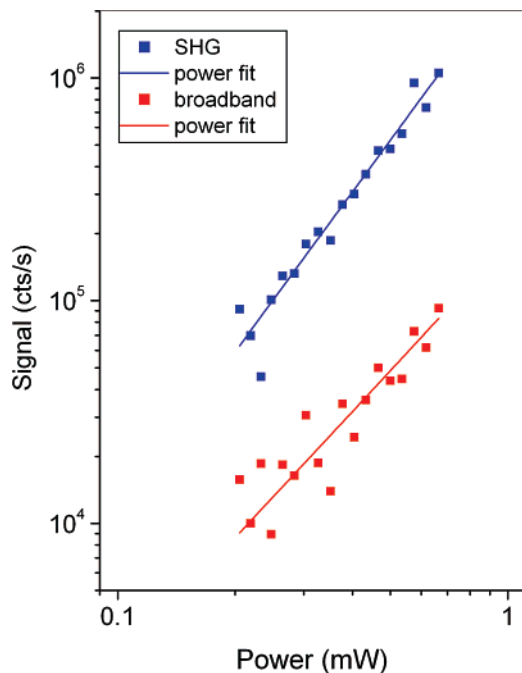
Figure 6. Emission intensity from the gap region vs pump power.
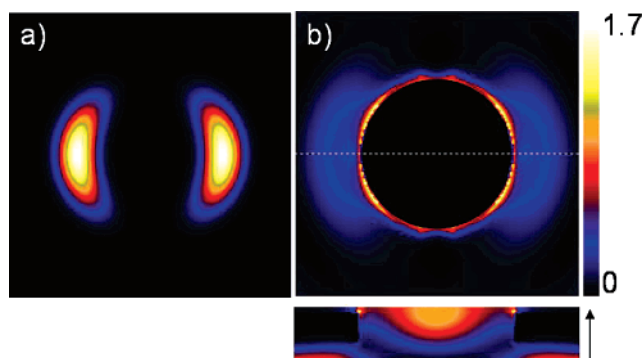
Figure 7. Models of single hole intensity maps. (a) A $(\sin \theta)^4$ function convoluted with a model point spread function for an ideal microscope. (b) FDTD calculated intensity map at 800 nm on the front face of the film for a single hole of 770 nm diameter. The regions where there is no film (inside the aperture) have been masked out because they are not expected to generate significant SHG. The dotted line corresponds to the cut used in the vertical cross-section below, and the arrow indicates the incident polarization direction of the laser.

Multiphoton absorption by roughened noble metal surfaces[29] and from resonant noble metal nanostructures[2,3,32] does lead to enhanced broadband emission. Furthermore, this emission is more sensitive to field enhancements than photoluminescence by single-photon excitation. Because the field enhancements are strongest near the metal surface, multiphoton-induced emission from the surface atoms may dominate over that from the bulk. This implies that field-enhancement effects are easier to measure with multiphoton excitation than with single-photon excitation.

The mechanism invoked for broadband emission continuum from bowtie antennas[3] involves two-photon interband excitation of electrons from the d band to the sp band followed by fast nonradiative recombination and plasmon
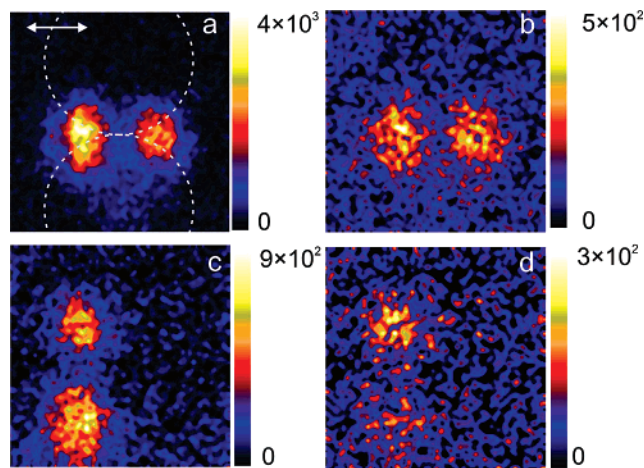
Figure 8. SHG and broadband continuum emission from a pair of adjacent 771 nm diameter apertures in a 100 nm thick Al film (1 μm $\times$ 1 μm scan). (a) SHG, polarization along the cusp line. (b) Broadband, polarization along the cusp line. (c) SHG, polarization orthogonal to the cusp line. (d) Broadband, polarization orthogonal to the cusp line.

emission. These plasmons subsequently radiate, giving rise to the enhanced photoluminescence.[31] Two-photon excited photoluminescence (TPPL) should hence be characterized by a quadratic dependence on the power at the fundamental frequency and should depend on the existence of plasmon resonances. The reasonable quadratic fits in Figure 5 suggest that TPPL is dominating the broadband emission from our cusp antennas, as well. However, when aluminum was used instead of gold, a weak broadband continuum signal from the structure was still observable, especially when the incident polarization was aligned with the cusp line, Figure 8. No signal (SHG or broadband) could be measured from the Al film.

To examine whether the observed emission is a multiphoton or single-photon effect, we have switched the laser from pulsed to a CW mode while maintaining the same average power. No luminescence could be measured in this case. Even when the CW power was raised very close to the damage threshold for Al (5 mW), we could not detect any luminescence coming from the structure or the film. The observed broadband emission is thus a multiphoton effect. Al has no interband transitions accessible by two-photon absorption at 800 nm. Therefore, the observed weak broadband emission from Al must have a physical origin different from TPPL.

Mühlschlegel et al. have studied the broadband continuum emitted by dipole optical antennas made of gold and concluded that it is due to white-light supercontinuum (WLSC) from the substrate glass, which is a fourth-order nonlinear phenomenon found in various dielectric materials.[2] Because the peak power densities in the present paper are ~10 times larger than those used in ref 2, WLSC could be an explanation for the observed broadband emission from Al. Unfortunately, our present setup and the weak emission when Al is used do not allow us to measure the signal dependence on the input laser power over a significant power range and elucidate the emission's physical origin.
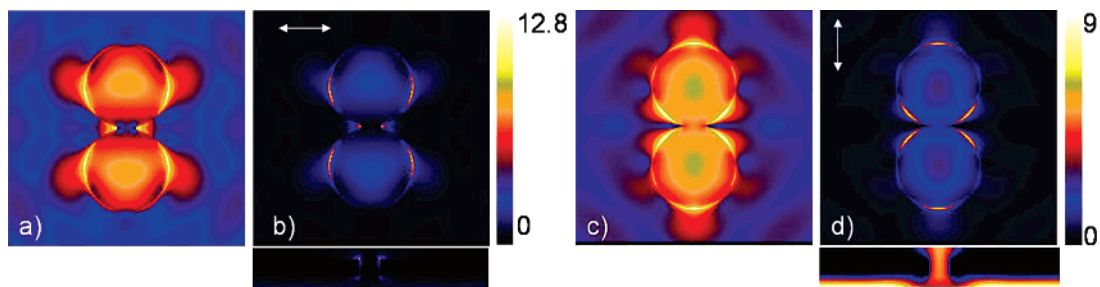
Figure 9. Calculated intensity maps at 800 nm from the front face of the film: (a and b) correspond to the case when the incident polarization was oriented along the cusp line; (a) uses a logarithmic color map to allow the visualization of the weaker fields on the perimeter of the double-hole structure, (b) uses a linear color scheme. A vertical cross-section containing the cusp line is given below (b). (c and d) Same as (a and b), but for an incident polarization perpendicular to the cusp line. Numerical values represent the ratio between the local field intensity and the incident one.

Another possible explanation for the presence of broadband emission with Al could be luminescence from adsorbates. However, when adsorbates are involved, there is usually a detectable change in the signal at the turning on of the laser beam due to desorption and rearrangement of the adlayer. We have not observed any initial transients in the SHG signal during laser exposure. Adsorbate involvement is therefore unlikely.

Note that the broadband emission with Al is 3 orders of magnitude weaker than the broadband luminescence from Au, which also includes TPPL. Therefore, while WLSC generation is probably present in Au, too, in this case, TPPL is the dominating contribution to the broadband continuum, hence the quadratic dependence in Figure 5.

Interestingly, a supraquadratic dependence is observed for SHG emitted from the cusps. Such behavior has been observed on films and explained previously by the interaction of the leading edge of a laser pulse with gold to create a nonequilibrium electron distribution.[33] The susceptibility producing SHG then depends on the nonequilibrium photo-excited electron concentration, which adds further nonlinearity. Supraquadratic SHG dependence is expected at laser intensities greater than 10^{10} W/cm². In our case, the peak incident laser intensity is ~10^{11} W/cm², which will be enhanced by structural resonances as discussed below. Recently, a similar modification of the nonlinear optical response has been reported for metallic subwavelength hole arrays.[34]

To understand the patterns and enhancements observed, we have performed further FDTD calculations. Figure 9 shows some results for a 100 nm thick Au film on glass with 770 nm diameter apertures and a 200 nm gap between the cusps. The calculated intensity maps at $\lambda = 800$ nm correspond to the front face of the film (on which the laser is incident). The two hot spots in Figure 9b cannot be resolved by the scanning confocal microscope because they are closer (~200 nm) than the resolution limit of the microscope (~285 nm). This is why Figure 3b shows a central spot with a maximum between the cusps. However, when the polarization is rotated to perpendicular to the cusp line, the most intense fields on both sides of each tip are located ~400 nm apart, therefore resolvable by the microscope. This explains the two distinct spots on the experimental maps for this case.

The calculated ratio between the maximum intensities for parallel and perpendicular polarization is 1.42, Figure 9. Assuming that most of the SHG signal is coming from the front surface, we expect a ratio between the maximum SHG signal for parallel and perpendicular polarizations of $(1.42)^2 = 2.01$. The experimental value obtained from Figure 2 is 1.8, in good agreement with the calculation.

If the optical response is dominated by local properties (as suggested by a quick comparison of Figure 2 and Figure 7a), one would expect for a hole pair a much larger enhancement of the field close to a tip when the polarization is along the tip axis than when it is perpendicular to it.[35] However, this is not what we observe in both experimental and simulation data of Figures 4 and 9: the "hot spots" for the different polarizations emit light of comparable intensity. Moreover, in Figure 9, there is clear evidence of standing waves around the holes' circumference, and the intensity profiles are quite different from those of a single hole, Figure 7b. This suggests that a quantitative explanation of the observed relative signal intensities requires considering contributions from shape resonances of the entire structure. We hypothesize that, as a function of wavelength, these resonances should modulate both the optical transmission and the local field enhancement.

We have performed an FDTD calculation to obtain the spectral transmission of a pair of holes across a broad range of wavelengths: 0.6−6 μm. To calculate transmission, we have integrated the far-field Poynting vector over the angular range (135°) corresponding to the NA of the objective and divided it by the value of the Poynting flux incident on the hole pair. Figure 10 gives the spectral transmission of an adjacent pair of holes, which shows indeed a strong resonance in the mid-IR region. The calculated maximum intensity enhancement factor at the cusps corresponding to this resonance exceeds 2500 for a gap of 200 nm. This enhancement corresponds to the fundamental (dipolar) mode of oscillation for the structure, Figure 10. Note that although T and E^2 vary in different ways, shape resonances are involved and both transmission and local field enhancement should be considered in future investigations of these antennas.

Across the entire spectral range under study, the maximum calculated enhancements predict local peak intensities in excess of ~10^{12} W/cm², well within the supraquadratic SHG
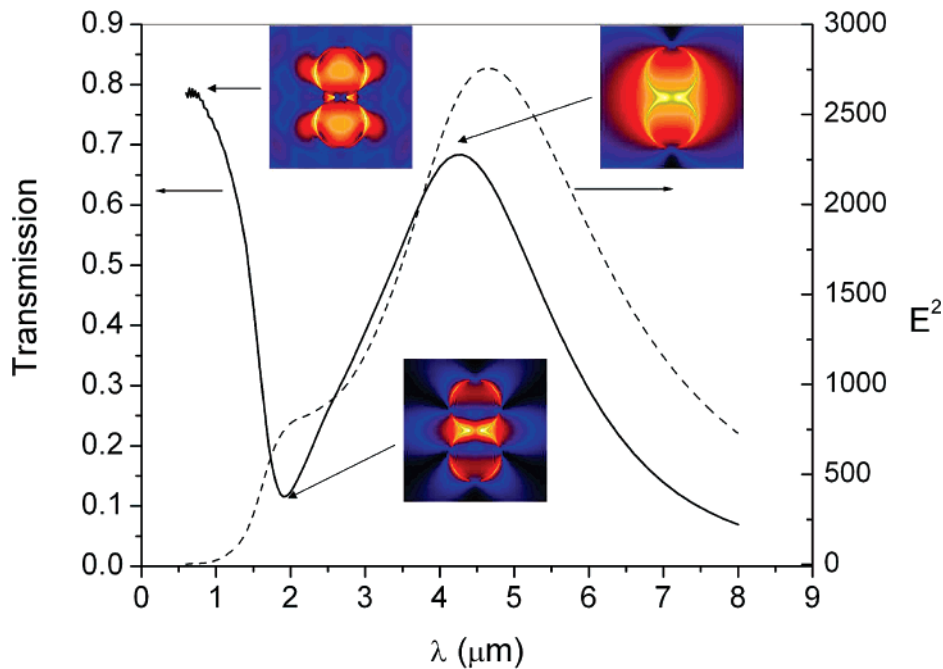
Figure 10. Calculated spectral transmission (left arrow) and maximum field intensity (right arrow) on the front face of the film from a pair of 770 nm holes (200 nm gap at the cusp) and logarithmic intensity maps corresponding to the wavelengths indicated by arrows (the color scale of the maps are different). The incident polarization is along the cusp line.

region observed by Moore and Donnelly,[33] which may explain the deviation observed in the analysis of the SHG dependence on the input power from a cusp, but not from a film.

The resonance location in the mid-IR scales with the hole diameter. Thus, this type of antenna may prove useful for molecular spectroscopy and chemical imaging applications.

To bring the resonance closer to the spectral range of our experimental setup and compare the predicted and the experimental spectral transmission, we collected data from pairs of holes 350 ± 20 nm in diameter with a 180 nm gap between tips and also performed calculations for a pair of 320 nm holes forming cusps with a 192 nm gap. These smaller holes have resonances nearer the visible range of the spectrum. The experimental data agrees well with the simulation over the spectral range of our apparatus, Figure 11.

Conclusions. Field-enhancement effects that arise near cusps between adjacent apertures in metal films have been studied with nonlinear optical microspectroscopy. Enhancements in broadband emission and SHG have been measured and good agreement has been found with FDTD computations. The magnitude of the relative changes in the nonlinear optical signal from the cusp structure at different polarizations suggest a mechanism involving surface modes running around the hole circumference. Numerical simulations show that significant field enhancements could be generated in IR, where the fundamental oscillation mode of the cusp antenna occurs. The SHG emitted by the cusp structure is characterized by a supraquadratic power dependence, while the SHG emitted from the film surrounding the structure exhibits the normal quadratic power dependence. For the first time, multiphoton-excited broadband emission has also been found
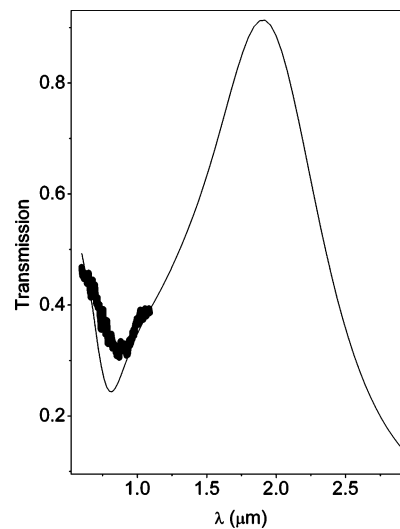
Figure 11. Experimental (dots) and simulated (line) spectral transmission of a pair of adjacent holes in a gold film. The light polarization is oriented along the cusp line.

to occur from cusp antennas made in aluminum films. This suggests that other mechanisms besides TPPL may contribute to the broadband emission.

References

(1) Crozier, K. B.; Sundaramurthy, A.; Kino, G. S.; Quate, C. F. *J. Appl. Phys.* **2003**, *94*, 4632−4642.

(2) Muhlschlegel, P.; Eisler, H. J.; Martin, O. J. F.; Hecht, B.; Pohl, D. W. *Science* **2005**, *308*, 1607−1609.

(3) Schuck, P. J.; Fromm, D. P.; Sundaramurthy, A.; Kino, G. S.; Moerner, W. E. *Phys. Rev. Lett.* **2005**, *94*, 017402.

(4) Aizenberg, J.; Rogers, J. A.; Paul, K. E.; Whitesides, G. M. *Appl. Phys. Lett.* **1997**, *71*, 3773−3775.

(5) Melville, D. O. S.; Blaikie, R. J. *J. Vac. Sci. Technol., B* **2004**, *22*, 3470−3474.

(6) Sundaramurthy, A.; Schuck, P. J.; Conley, N. R.; Fromm, D. P.; Kino, G. S.; Moerner, W. E. *Nano Lett.* **2006**, *6*, 355−360.

(7) H'Dhili, F.; Bachelot, R.; Lerondel, G.; Barchiesi, D.; Royer, P. *Appl. Phys. Lett.* **2001**, *79*, 4019−4021.

(8) Blaikie, R. J.; Melville, D. O. S. *J. Opt. A: Pure Appl. Opt.* **2005**, *7*, S176−S183.

(9) Anderson, M. S. *Appl. Phys. Lett.* **2000**, *76*, 3130−3132.

(10) Demming, A. L.; Festy, F.; Richards, D. *J. Chem. Phys.* **2005**, *122*, 184716.

(11) Michaels, A. M.; Jiang, J.; Brus, L. *J. Phys. Chem. B* **2000**, *104*, 11965−11971.

(12) Novotny, L. Forces in optical near-fields. In *Near-Field Optics and Surface Plasmon Polaritons*; Springer-Verlag: New York, 2001; Vol. 81, pp 123−141.

(13) Ganic, D.; Gan, X. S.; Gu, M. *Opt. Express* **2004**, *12*, 5533−5538.

(14) Kwak, E. S.; Onuta, T. D.; Amarie, D.; Potyrailo, R.; Stein, B.; Jacobson, S. C.; Schaich, W. L.; Dragnea, B. *J. Phys. Chem. B* **2004**, *108*, 13607−13612.

(15) Chaumet, P. C.; Rahmani, A.; Nieto-Vesperinas, M. *Phys. Rev. B* **2005**, *71*, 045425.

(16) Grober, R. D.; Schoelkopf, R. J.; Prober, D. E. *Appl. Phys. Lett.* **1997**, *70*, 1354−1356.

(17) Compton, R. C.; McPhedran, R. C.; Popovic, Z.; Rebeiz, G. M.; Tong, P. P.; Rutledge, D. B. *IEEE Trans. Antennas Propag.* **1987**, *35*, 622−631.

(18) Fromm, D. P.; Sundaramurthy, A.; Schuck, P. J.; Kino, G.; Moerner, W. E. *Nano Lett.* **2004**, *4*, 957−961.

(19) Sundaramurthy, A.; Crozier, K. B.; Kino, G. S.; Fromm, D. P.; Schuck, P. J.; Moerner, W. E. *Phys. Rev. B* **2005**, *72*, 165409.

(20) Jin, E. X.; Xu, X. F. *Appl. Phys. Lett.* **2006**, *88*, 153110.

(21) Lesuffleur, A.; Kumar, L. K. S.; Gordon, R. *Appl. Phys. Lett.* **2006**, *88*, 261104.

(22) Haynes, C. L.; Van Duyne, R. P. *J. Phys. Chem. B* **2001**, *105*, 5599−5611.

(23) Amarie, D.; Rawlinson, N. D.; Schaich, W. L.; Dragnea, B.; Jacobson, S. C. *Nano Lett.* **2005**, *5*, 1227−1230.

(24) Taflove, A. *Computational Electrodynamics: The Finite Difference Time-Domain Method*; Artech House: Norwood, MA, 1995.

(25) Palik, E. D. *Handbook of Optical Constants of Solids*; Academic Press: New York, 1997.

(26) Chang, S. H.; Gray, S. K.; Schatz, G. C. *Opt. Express* **2005**, *13*, 3150−3165.

(27) Levene, M. J.; Korlach, J.; Turner, S. W.; Foquet, M.; Craighead, H. G.; Webb, W. W. *Science* **2003**, *299*, 682−686.

(28) Mooradian, A. *Phys. Rev. Lett.* **1969**, *22*, 185−187.

(29) Boyd, G. T.; Yu, Z. H.; Shen, Y. R. *Phys. Rev. B* **1986**, *33*, 7923−7936.

(30) Wilcoxon, J. P.; Martin, J. E.; Parsapour, F.; Wiedenman, B.; Kelley, D. F. *J. Chem. Phys.* **1998**, *108*, 9137−9143.

(31) Dulkeith, E.; Niedereichholz, T.; Klar, T. A.; Feldmann, J.; von Plessen, G.; Gittins, D. I.; Mayya, K. S.; Caruso, F. *Phys. Rev. B* **2004**, *70*, 205424.

(32) Bouhelier, A.; Beversluis, M. R.; Novotny, L. *Appl. Phys. Lett.* **2003**, *83*, 5041−5043.

(33) Moore, K. L.; Donnelly, T. *Opt. Lett.* **1999**, *24*, 990−992.

(34) van Nieuwstadt, J. A. H.; Sandtke, M.; Harmsen, R. H.; Segerink, F. B.; Prangsma, J. C.; Enoch, S.; Kuipers, L. *Phys. Rev. Lett.* **2006**, *97*, 146102.

(35) Novotny, L.; Bian, R. X.; Xie, X. S. *Phys. Rev. Lett.* **1997**, *79*, 645−648.